Mechanical regains due to self-healing in cementitious materials: Experimental measurements and micro-mechanical model

Benoit Hilloulin, Damien Hilloulin, Frederic Grondin, Ahmed Loukili, Nele de Belie

Mechanical regains due to self-healing in cementitious materials: Experimental measurements and micro-mechanical model

Benoit Hilloulin [a,b], Damien Hilloulin [c], Frédéric Grondin [a], Ahmed Loukili [a,*], Nele De Belie [b]

[a] LUNAM Université, Institut de Recherche en Génie Civil et Mécanique (GeM), UMR-CNRS 6183, Ecole Centrale de Nantes, 1 rue de la Noë, 44321 Nantes, France
[b] Magnel Laboratory for Concrete Research, Ghent University, Technologiepark Zwijnaarde 904, B-9052 Ghent, Belgium
[c] Supélec Sciences des Systèmes, EA4454 (E3S), 3 rue Juliot-Curie, 91192 Gif sur Yvette Cedex, France

This paper focuses on mechanical regains that can be obtained due to self-healing of cementitious materials. Experimentally, small cracks with a width of around 10 μm were healed by water immersion and corresponding regains were assessed by means of three-point-bending tests. A general discussion about stiffness and strength regains is provided with the help of newly introduced indices. Besides, the first comprehensive finite element model to characterise the micro-mechanical properties of the healing products is introduced, based on the coupling of the microstructural hydration model CEMHYD3D and the finite element code Cast3M. The main objective is to analyse the healing potential and rate, as well as the nature of the healing products. The nature of the simulated healing products is in agreement with observation conducted using SEM/EDX on artificial cracks created at early age.

1. Introduction

Cracks in concrete generate massive inspection and repair costs. Self-healing of concrete could be a means to considerably decrease these costs by increasing impermeability and/or restoring mechanical properties of a damaged structure [1]. Concrete's intrinsic ability to heal, called autogenic healing [2], has been reported for many years and its discovery is attributed to the French Academy of Sciences. This natural process is being improved and supplemented for some years by promising engineered additions such as mineral additions [3], capsules containing healing agents [4–7], minerals producing bacteria [8–10] or fibres limiting the crack width [11–15]. Development of non-destructive monitoring techniques facilitates the assessment of self-healing efficiency, both for natural or engineered healing [16–19].

Two main mechanisms are considered predominant in autogenic healing: calcite or portlandite (CH) precipitation following calcium leakage into the crack, and further hydration triggered by water ingress into the crack [20,21]. These two mechanisms can occur together at the same time [22] but their extent likely depends on the age and composition of concrete (amount of anhydrous clinker) [23,24]. Further hydration and portlandite precipitation into the crack can lead to tensile strength regains [24], compression strength regains [25–27] and bending strength regains [28,29]. Stiffness regain can also be obtained at the same time [29]. Up to now, many studies show that mechanical regains are slow and immersion into water for several weeks is needed [29,30]. Moreover, most of the studies have been carried out on mature concrete, and did not investigate the healing potential of concrete cracked at early age while it can lead to better regains [24,31] and it could have practical implications concerning plastic or drying shrinkage cracks created some hours after setting. On the other hand, recent observations and models state that the healing phenomenon has a relatively high speed during the first dozens of hours [22,23], both for calcite and hydrate formation. However, the relative importance and the kinetics of these phenomena should be better understood in order to increase autogenous self-healing capabilities of concrete.

In order to develop autogenous healing and associated mechanical regains, numerical models could help design and optimise concrete's formulation. Several tools have been developed over the last decades to model microstructural evolution of concrete/mortar/cement paste over time from hydration to degradation. Modelling codes like CEMHYD3D simulating concrete hydration [32], can lead to good estimations of mechanical properties [33,34]. Few models were developed to describe self-healing of concrete. Some models were proposed to determine the amount of unhydrated cement particles in concrete specimens considering w/c ratio and cement fineness which underlies the self-healing potential [31,35,36], or to calculate the amount of healing product due to further hydration considering two crack modes [37,38]. Recently, a model simulating further hydration using water transport theory, ion diffusion theory and thermodynamics theory has been developed to determine the evolution of the filling fraction of cracks [22,39,40]. However, these models do not provide any information about the mechanical effects of self-healing. At a mesoscale, models assigning new properties to the healing products have been introduced

* Corresponding author.
E-mail address: ahmed.loukili@ec-nantes.fr (A. Loukili).

through the use of lattice models [31,41] or interface elements [42]. A mesoscopic finite element model giving mechanical information about the distribution and the intrinsic properties of the healing products has been proposed [43] but does not provide a description of the self-healing development and its mechanical influence at a microscale, and there is a need for multiscale modelling from microscale [44] as for hydrating systems [45]. Regarding the limitations of the current models and the reproducibility of the experiments, coupled approaches, combining modelling and experimental work are useful to get a better understanding of the phenomenon.

Thus, to contribute to answering these questions, mechanical regains due to healing by ongoing hydration are investigated in this study using both experimental and modelling methods. Experimental works are conducted on specimens cracked at early age to investigate their healing potential according to various parameters (e.g. healing time, initial crack width and age at cracking). A focus is put on the minimum time to obtain mechanical regains for a given crack width in order to explain the development of the healing phenomenon. Also, the origin of the difference between stiffness and strength is investigated. Some SEM/EDX observations made on artificial planar cracked cement paste are presented in order to support the three-point bending tests results and give precise information concerning the nature of the healing products. Besides, a first micro-mechanical model for self-healing in cementitious materials is introduced. Healing by further hydration is simulated using our modified version of CEMHYD3D called CemPP to understand the kinetics and the potential of the healing phenomenon for different crack widths, age at cracking and healing period duration. The microstructure of healed specimens then served as input to the finite element code Cast3M [46] to monitor the mechanical regains and provide explanations for some experimental observations. This coupling has been made possible by extending the CEMHYD3D code to run different independent modules, each one providing part of the information necessary to the coupling with Cast3M, or directly operating on the microstructure.

2. Materials and experiments

2.1. Materials and sample preparation

Mortar was prepared with CEM II A-LL 42.5 R CE PM CP2 NF and 0/2 mm sand with the following proportions: 1250 kg/m^3 of sand, 755 kg/m^3 of cement, 265 kg/m^3 of water and a mass of superplasticizer (ChrysoFluid Optima 206, dry matter of 20%) representing 0.5% of the cement mass.

Mortar prisms with dimensions of $7 \times 7 \times 28$ cm^3 were cast. After 1 day of curing under sealed conditions in an air-conditioned room at a temperature of 20 °C, the specimens were demoulded (except the specimens cracked at 10 h which were demoulded at 10 h). A notch 7 mm deep and 5 mm wide was cut at the centre of all beams in order to initiate cracking at a specific location using three-point bending test. The specimens were then kept stored in tap water at a temperature of 20 °C before cracking and during the healing period. After the healing period, the healed and the reference specimens were reloaded after 2–3 h exposure to room temperature necessary for the Crack Mouth Opening Displacement (CMOD) dispositive preparation.

Complementarily, artificially cracked cement paste samples were prepared using the same cement to determine the extent and the composition of the healing products similarly to what has been done in [22]. The principal interest of this technique is that a precise distinction between the healing products and the original matrix can be obtained, which is not the case for post-observation of healed cement paste or mortar specimens containing realistic cracks. To prepare the samples, 2 parallelepipeds of cement paste with dimension of 15 mm × 15 mm × 30 mm were sawn and 2 adjacent faces with a length of 30 mm were polished using silicon carbide paper and diamond spray (down to 1 μm). In order to correspond to the cracking dates of the mortar specimens, artificial planar cracks with a width of around 20 μm were then created at the age of 1, 3 and 7 days by gluing 2 parallelepipeds together as illustrated in Fig. 1. Specimens were then immersed for 3 days to 4 weeks to heal. They were removed after the healing period and briefly polished on one of the initially polished sections before being investigated with SEM/EDX using an acceleration voltage of 20 kV ensuring a rather small penetration of the X-rays into the sample.

2.2. Quantification of mechanical regains due to healing

In order to evaluate the mechanical regains due to self-healing, specimens were pre-cracked, up to different levels of residual crack opening (CODi) employing the three-point bending test set-up controlled by CMOD. Some specimens were kept uncracked for reference. The real crack width was measured using an optical microscope at the bottom part of the beams as described in [16]. In this study, we focused on the influence of the age at cracking, the crack width and the healing time. A synopsis of the experimental programme is presented in Table 1.

After the healing period, the specimens subjected to healing were reloaded in order to determine their stiffness and their strength (resp. K_{healed} and F_{healed}). At the same time, the reference specimens of the same age were subjected to the three-point-bending test. A first load was applied to determine their initial stiffness and strength (resp. K_{ref} and F_{ref}), then they were unloaded to obtain the residual crack opening CODi defined for the healed specimens. The reference specimens were then reloaded immediately to determine their residual stiffness and strength (resp. $K_{unhealed}$ and $F_{unhealed}$) which could represent the parameters of unhealed specimens according to some studies [29,30]. The different quantities of interest are represented in Fig. 2. Several indices can be calculated to represent the healing efficiency, taking into account the brittle behaviour of the healed specimen [26]:

- K_{healed}/K_{ref} and F_{healed}/F_{ref} which can be compared resp. to $K_{unhealed}/K_{ref}$ and $F_{unhealed}/F_{ref}$,
- the index of load recovery with regard to the reference ILRref and the index of damage recovery with regard to the reference IDRref, which are similar to indices previously introduced [3]. These indices are defined by Eqs. (1) and (2). ILRref and ILKref vary between 0 (no healing) and 1 (perfect healing).

$$ILRref = \frac{F_{healed} - F_{unhealed}}{F_{ref} - F_{unhealed}} \quad (1)$$

$$IDRref = \frac{K_{healed} - K_{unhealed}}{K_{ref} - K_{unhealed}} \quad (2)$$

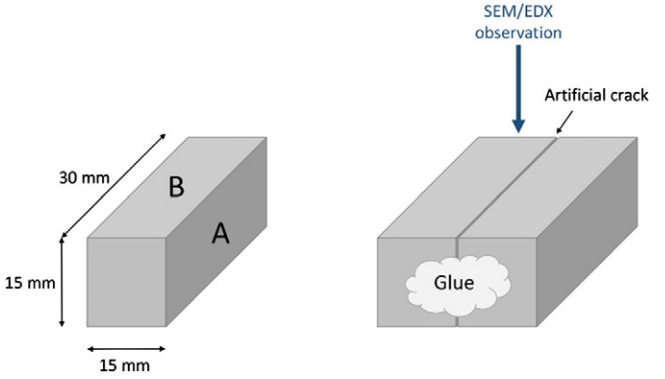

Fig. 1. Schematic diagram of the preparation on artificial cracks for SEM investigation. A and B denote the initially polished surfaces.

Table 1
Synopsis of the experimental programme.

Specimen name	Age at cracking	CMOD before unloading (corresponding average real crack width) (μm)	Healing time
S1	24 h	35 (10)	2 weeks
S1-5 m	24 h	25 (5)	2 weeks
S1-20 m	24 h	45 (20)	2 weeks
S1-72 h	72 h	35 (10)	2 weeks
S1-7d	7d	35 (10)	2 weeks
S1-h2d	24 h	35 (10)	2 days
S1-h7d	24 h	35 (10)	7 days
S1-h5w	24 h	35 (10)	5 weeks

3. Numerical assessment of mechanical regains at microscopic scale

3.1. Presentation of CemPP, a modified version of CemPy

To be able to develop easily our coupling method, and also in the consideration of trying to eventually model new reactions, we decided to add to CemPy 0.15 [47] the possibility for the user to run his own 'transformation passes' on the microstructure. The transformation passes must be coded as C++ classes implementing a given interface, thus the version we developed is called CemPP. The transformation passes have a full access to the whole simulation state from this interface. These transformation passes can be as simple as just replacing some chemical species in a given region by other species (e.g. removing phases to create a crack), to perform some analysis (e.g. measure the size of the pores in the structure, get a report of the chemical structure), or to trigger external programmes to realize some coupling. These transformation passes are programmed through a GUI or configuration files to be enabled/disabled at specific time points (given in hours), and at a certain frequency (number of simulation cycles between two executions of the same pass).

3.2. Microstructure generation using a CEMHYD3D-based platform

Generation of microstructure until the age of cracking was realized using CemPP with a discretization of 1 μm over a volume of 100 μm. Model hydration is carried out via cycles of dissolution, diffusion, and reaction, according to known reaction equations. The correct volumetric stoichiometry is maintained throughout the hydration modelling process. Induction time (t_0) and calibration factor (β) for converting model cycles to real time in hours were taken equal to 4 hours and 0.0005 to give an approximate kinetic to the hydration process:

$$time = t_0 + \beta \times cycle^2. \quad (3)$$

Real particle size distribution of cement grains measured by laser diffraction is input to build the corresponding distribution in the model. Other major inputs for CemPP are detailed in Table 2. The composition of the cement is the same as the one given by the supplier.

3.3. Healing by further hydration

At the time corresponding to the experimental age of cracking, an artificial crack was generated in the microstructure in order to numerically study the healing process of this crack by ongoing hydration. A plane crack with a given width was realized by replacing a part of the microstructure by void using a dedicated pass. Then, the hydration process was restarted, filling the crack and the surrounding empty pores by water, using another pass after each hydration cycle, to simulate healing of this crack by precipitation of hydration products in the crack. Dissolution and precipitation probabilities have not been changed in order to see whether normal hydration rates and products can justify experimental observations. An example of the healing process, e.g. filling of the crack by hydration products, is given in Fig. 3.

Along the healing process, CemPP outputs were analysed to determine the solid phases formed around the crack and make a comparison with the inner cement paste. This analysis was carried out on the entire microstructure outputs from the healing-by-ongoing-hydration model after different healing periods selected to correspond to the experimental healing periods.

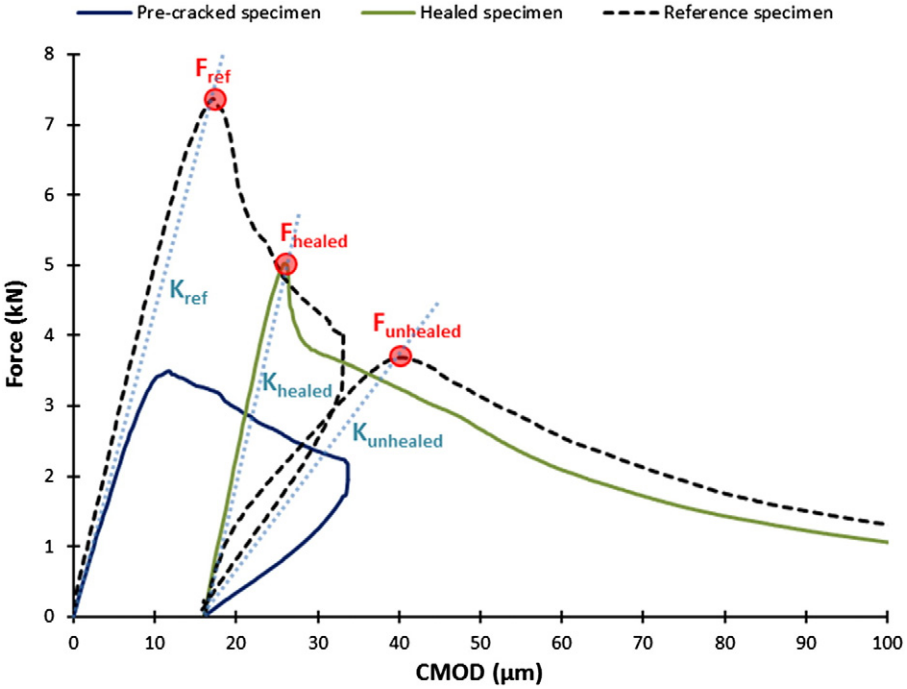

Fig. 2. Example of Load vs. CMOD curves for specimens submitted to healing and reference specimens; definition of quantities for calculation of self-healing indices.

Table 2
CemPP inputs for the hydration model.

Blaine fineness	380 m^2/kg
Gypsum dihydrate	5% vol.
C_3S	67.2 mass %
C_2S	8.8 mass %
C_3A	7.3 mass %
C_4AF	11.1 mass %
Activation energy	33.5 kJ/mol
w/c	0.35
Initial temperature	20 °C
Curing conditions	Saturated

3.4. Mechanical properties of healed specimens

In order to study the mechanical regains due to healing, micromechanical tensile tests were performed on 3D subparts of the output microstructure. Finite element simulations were carried out on $20 \times 30 \times 10$ voxels volumes for 5-µm wide cracks, or $20 \times 30 \times 15$ voxels volumes for 10-µm wide cracks along the directions $\vec{e_1}$ (perpendicular to the crack), $\vec{e_2}$ and $\vec{e_3}$ (parallel to the crack). These subvolume sizes are trade-off between computational times, representability (size of the volume vs largest particles) and stability of the results (dependence to the location and a size increase of the subvolume). For more heterogeneous cement paste (including mineral additions like slag), subvolume dimensions should be sensibly larger. These subvolumes were deliberately chosen at the same location for all the specimens to follow the influence of the healing process, e.g. microstructural change

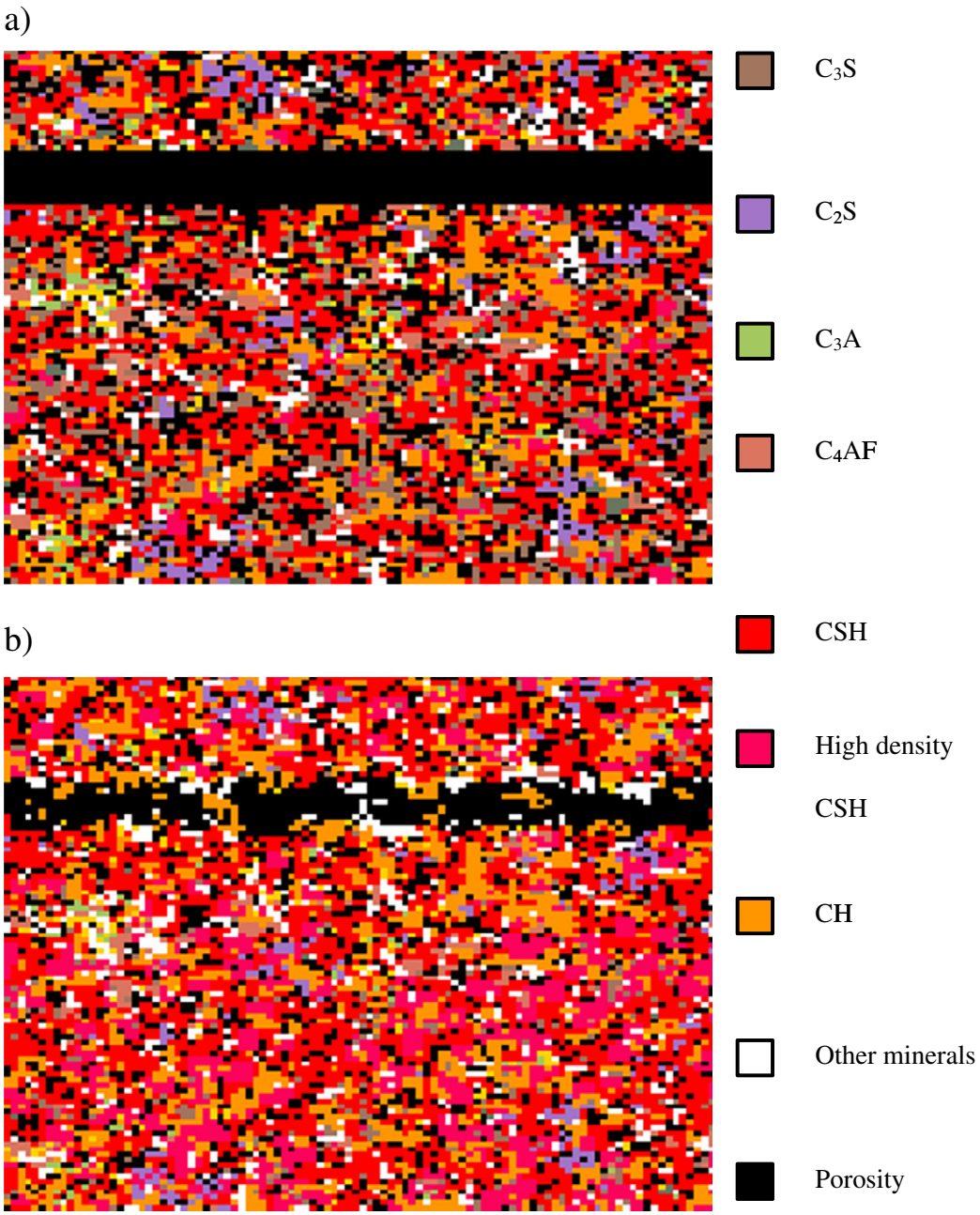

Fig. 3. Example of the healing process modelled using CEMHYD3D: a) 2D microstructural slice at 24 h just after the 10-µm wide crack creation, b) same microstructure after 194 h healing.

around the crack, on the mechanical behaviour. Young's modulus of the small volume, Y_1 and Y_2, were successively calculated, resp. along the two directions $\vec{e_1}$ and $\vec{e_2}$, resolving the classic elastic problem linking the overall stress σ, the overall displacement ε, the global displacement u and the global stiffness tensor C^i including all the individual local Young's moduli of the different phases (Eqs. (4) to (6)) given in Table 3 [34,48]. To do so, gradual displacements were applied on the external surfaces as boundary conditions. They are detailed in resp. Eqs. (7) and (8) referring to Fig. 4 for resp. the calculation of Y_1 and Y_2. Finally, the slope of the (σ, ε) curve represents the homogenised elastic Young's modulus Y_1 or Y_2.

$$div\,\sigma = 0 \tag{4}$$

$$\sigma = C^i : \varepsilon \tag{5}$$

$$\varepsilon = \frac{1}{2}(\nabla u + t\nabla u) \tag{6}$$

$$\varepsilon = \begin{cases} E_1\ on\ \Gamma_1 \\ 0\ elsewhere \end{cases} \tag{7}$$

$$\varepsilon = \begin{cases} E_2\ on\ \Gamma_2 \\ 0\ elsewhere \end{cases} \tag{8}$$

With the healing process Y_1, which is close to 0 after the creation of the crack, tends to Y_2. Then the ratio Y_1/Y_2 was chosen as a healing index: equal to 0 it corresponds to no tensile regains, while it tends to increase to 1 (or possibly more) as the number of healing products bridging the crack increases. An overview of the CemPP–Cast3M coupling is presented by Fig. 5.

4. Results and discussion

4.1. Experimental mechanical regains

Healing potential of the specimens was quantified analysing the loading curves of both the healed and the reference specimens as illustrated in Fig. 6, obtained for the different ages at cracking for specimens healed during 14 days. A relatively brittle fracture in the reloading curve, which can be attributed to self-healing, has been observed for the specimen cracked at 24 h. For all the specimens, mechanical regains were determined and the influence of the different parameters is discussed hereafter. Thus depending on the extent of the regains, different types of reloading curves can be obtained. In case of important regain (as for specimen cracked at 24 h on Fig. 6), regains are sufficient so that the peak load during reloading is higher than the peak load of the unhealed specimen. In case of smaller regain two-slopes reloading curves, which have been previously obtained for ultra-high performance concrete fractured at mature age and healed during several weeks [29] are observed (for specimens cracked at 72 h and 7 days on Fig. 6). These curves, typical of a stiffness regain with limited strength regain, indicate that the mechanical impact of the healing phenomenon can be compared for different types of mortar/concrete even if their composition is different. For some cases, a fast load drop was observed in the reloading curves as illustrated by specimen cracked at 7 days on Fig. 6. This could be due to the brittle behaviour of the healing products as hypothesised in [43] and eventually to the lower proportion of healing products, as this trend has generally been observed for specimens cracked at later age or with the largest crack width.

Table 3
Elastic moduli of individual cement and cement paste phases used in the simulation, taken from several sources in the literature reported in [34].

Mineral name	Cement chemistry notation	E (GPa)	ν	Ref.
Tricalcium silicate	C_3S	117.6	0.314	[49]
Dicalcium silicate	C_2S	Same as C_3S		[50]
Tricalcium aluminate	C_3A	Same as C_3S		[50]
Tetracalcium aluminoferrite	C_4AF	Same as C_3S		[50]
Calcium silicate hydrate	CSH	22.4	0.25	[50,51]
Portlandite	CH	42.3	0.324	[52]

4.1.1. Influence of the age at cracking

The age at cracking determines the healing potential. A good stiffness recovery has been achieved for the majority of the specimens (Fig. 7a) as already observed earlier [29]. The stiffness after healing can also be higher than the reference stiffness which can be explained by a better hydration in the uncracked zones because of the presence of a crack that facilitates water ingress. The later the cracks were created, the smaller were the bending strength regains. When the crack was created after 3 days, the mechanical regains were small and hardly quantifiable in the relatively short healing period of 14 days (Fig. 7b). For specimens cracked at 3 days, the small mechanical regains, e.g. strength ratio, should be attributed to the low $F_{unhealed}$ value of the reference specimen during reloading (see Fig. 6). One should immerse the specimens for a longer time, e.g. several weeks, to observe mechanical regains, which are often restricted [29,30]. When the cracks were created before 3 days, very good mechanical regains can be obtained, and even a complete regain in bending strength was observed for specimens cracked at 10 h (just after setting) but these results are not detailed here as the crack width measurement was relatively irregular and inferior to 10 μm at some locations.

4.1.2. Influence of the healing period

In this study, the focus is on the minimal healing period necessary to obtain mechanical regains in order to better understand the kinetics and the origin of the mechanical regains. Although higher mechanical regains should be obtained for longer healing periods and larger cracks could be healed, a better understanding of the healing at early stages for short healing periods could help to design faster healing techniques and represents more realistic conditions where fractured specimens are not constantly immersed into water.

Stiffness regain increases quickly during the first days of healing for all the specimens and stiffness is almost completely restored in 1 week when compared to the reference specimen (Fig. 8a). However, the minimum healing period to measure strength regain is between 1 week and 2 weeks for the cracks with an initial width of 10 μm (Fig. 8b). This time lag between the stiffness and the strength regains should indicate an increase of the mechanical properties of the healing product itself or an increase of the quantity of healing product bridging the crack over time, as it has already been characterised by a mesoscopic numerical analysis [43].

4.1.3. Influence of the crack width

For the three small crack widths studied (5, 10, 20 μm average real crack width), a complete stiffness regain can be achieved within 2 weeks of healing (Fig. 9a). However, the strength regain after a given healing time depends on the initial crack width. F_{healed}/F_{ref} decreases significantly while the width of the initial crack width increases (Fig. 9b).

To avoid any bias due to varying load levels used to create different crack widths, one should also compare the index of load recovery with regard to the reference ILRref and the index of stiffness recovery with regard to the reference IDRref. IDRref is higher than 1 for the three specimens which indicates a perfect stiffness recovery. ILRref is 0.61 for the 5-μm wide crack and drops to around 0.4 for the two other crack widths. This indicates that, for a given short healing time, the mechanical regains are much higher for the smaller crack width.

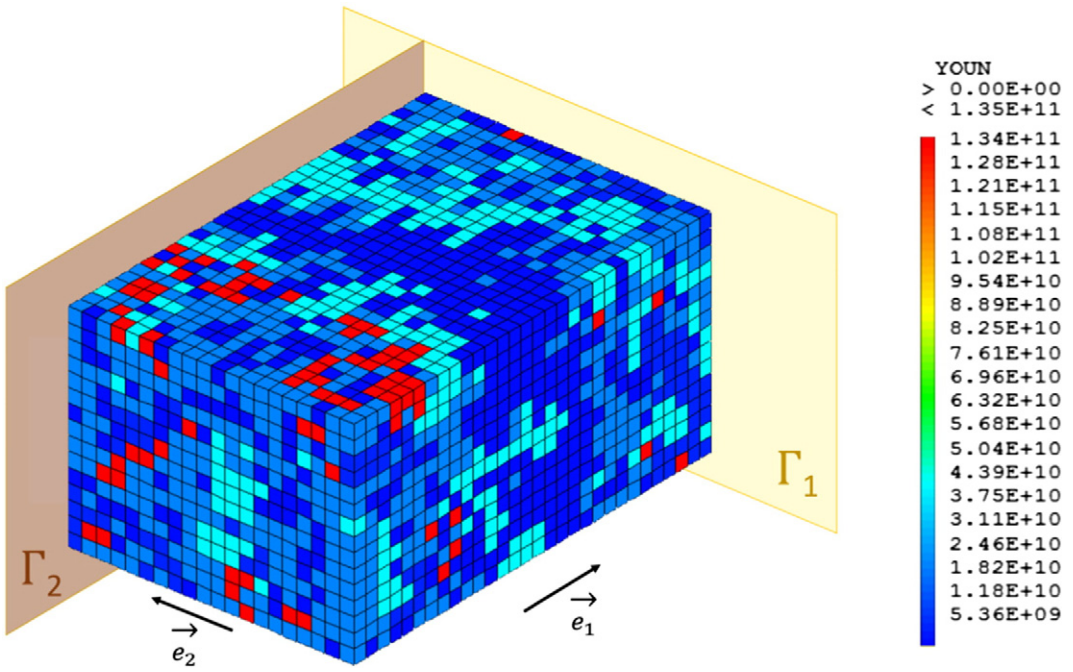

Fig. 4. Illustration of a subvolume used for finite element simulation of a specimen cracked at 24 h and healed 194 h. Crack is initially at the centre of the subvolume. Legend indicates Young's modulus, and planes Γ_1 and Γ_2 refer to boundary conditions.

4.2. Experimental observation of healing products

The major healing products observed are portlandite and CSH, as already reported by many researchers. However, healing products formed after early age cracking can include a high aluminium content as illustrated by Fig. 10, leading to CA(S)H phases formation. This high Ca/Si and Al/Si content can be due to the smaller diffusion rate of $H_2SiO_4^{2-}$ compared to Al^{3+} and Ca^{2+} [53]. One may also notice the size of the portlandite healing product formed after only 2 days healing.

For artificial cracks created after 3 days, this trend was not observed anymore and Al/Ca and Si/Ca ratios measured were close to, respectively 0 and 0 or 0.3 for portlandite and CSH, which is a composition that matches the composition of primary hydration products. The only difference between the healing products and the primary hydration products is therefore their aspect: portlandite generally presents a 'crystal-like' shape [22] while the CSH presents a more or less dense 'cloudy gel-like' aspect as illustrated in Fig. 11, similar to the one observed by [28]. Most of the time CSH healing products were located nearby an anhydrous clinker while no preferential precipitation location can be detected for portlandite.

Interestingly, for early cracking, long ettringite needle formation has been observed, mainly at the surface of the specimens along with some portlandite and calcite. These needle can completely fill large spaces like pore or cracks extremities (over-polished because of the edge effect)

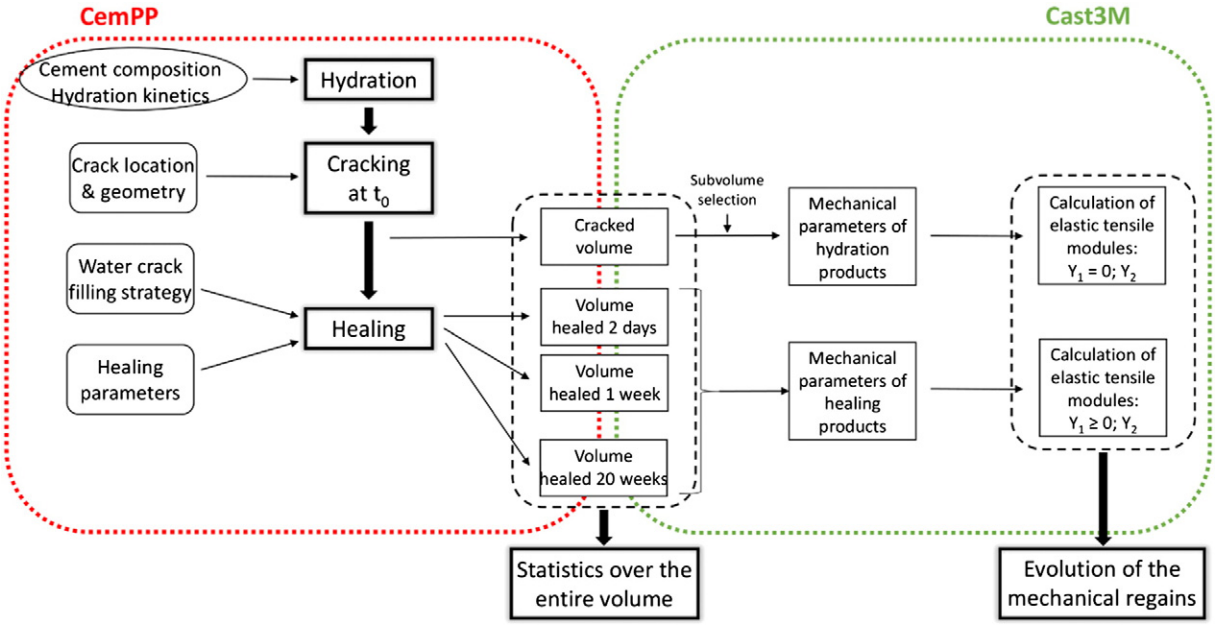

Fig. 5. Overview of the CemPP–Cast3M coupling.

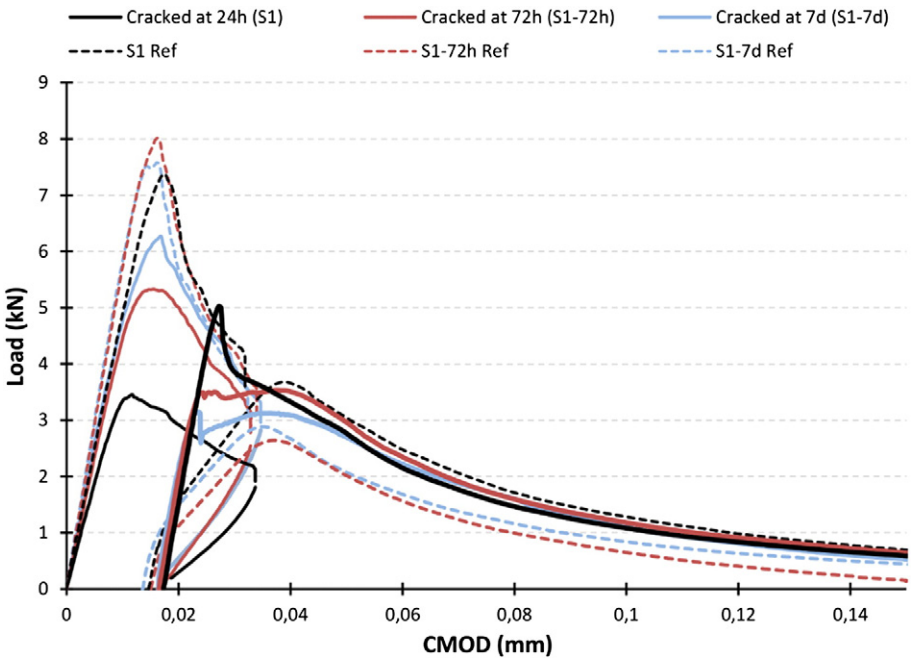

Fig. 6. Load vs CMOD curves obtained for specimens cracked at different ages, reloading curves of the healed specimens after 14 days (full lines) and loading and reloading curves of the respective reference specimens (dashed lines).

with a width close to 200 µm as illustrated by Fig. 12. Although some ettringite needles have been observed on latterly cracked specimens, their size and number were limited.

Despite the comparison between the healing products thickness and the crack width is rather complicated because of the low air pressure applied during SEM measurements which reopens the cracks, it seems that healing product CSH thickness cannot increase up to 20 µm within the first week. After 4 weeks of immersion, CSH bridging 20 µm-wide cracks was found.

In conclusion, the observation of healing products in artificial cracks created at different ages can supplement the measurement of the mechanical regains on mortars. First, development of portlandite and

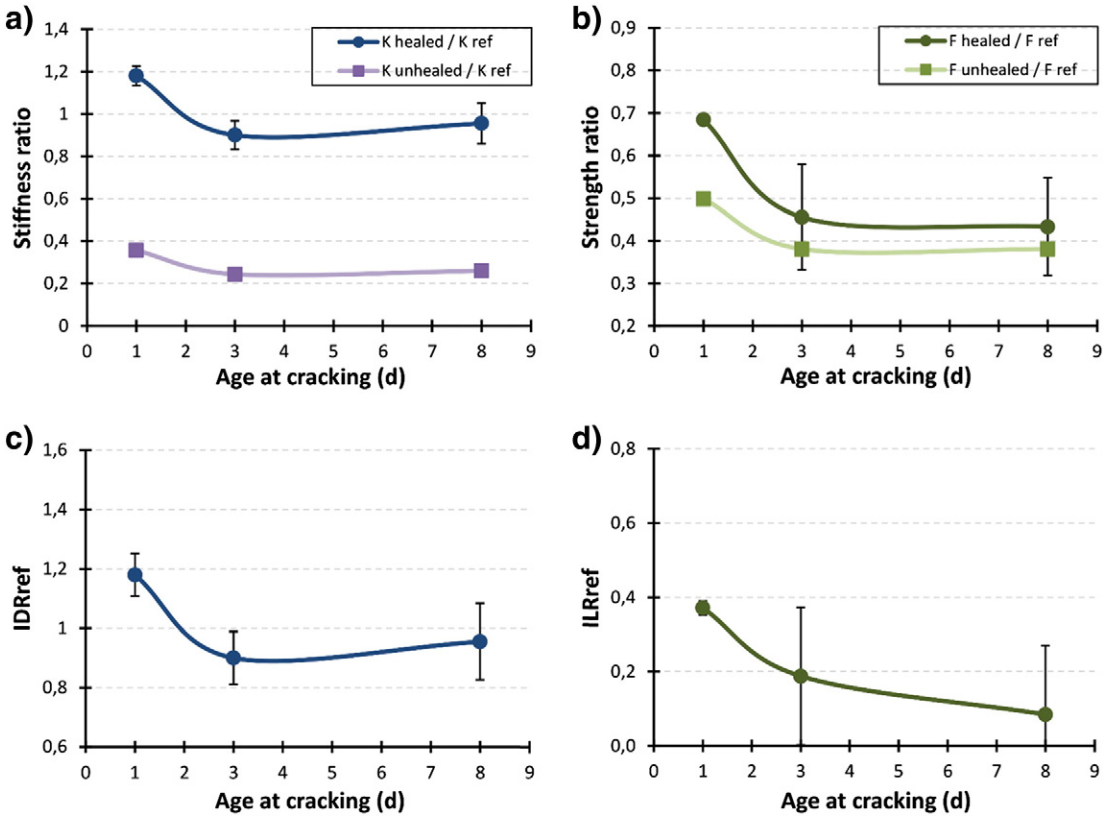

Fig. 7. Influence of the age at cracking for specimens with a 10-µm wide crack healed for 14 days, on a) the stiffness regain, b) the bending strength regain, c) the index of damage recovery and, d) the index of load recovery.

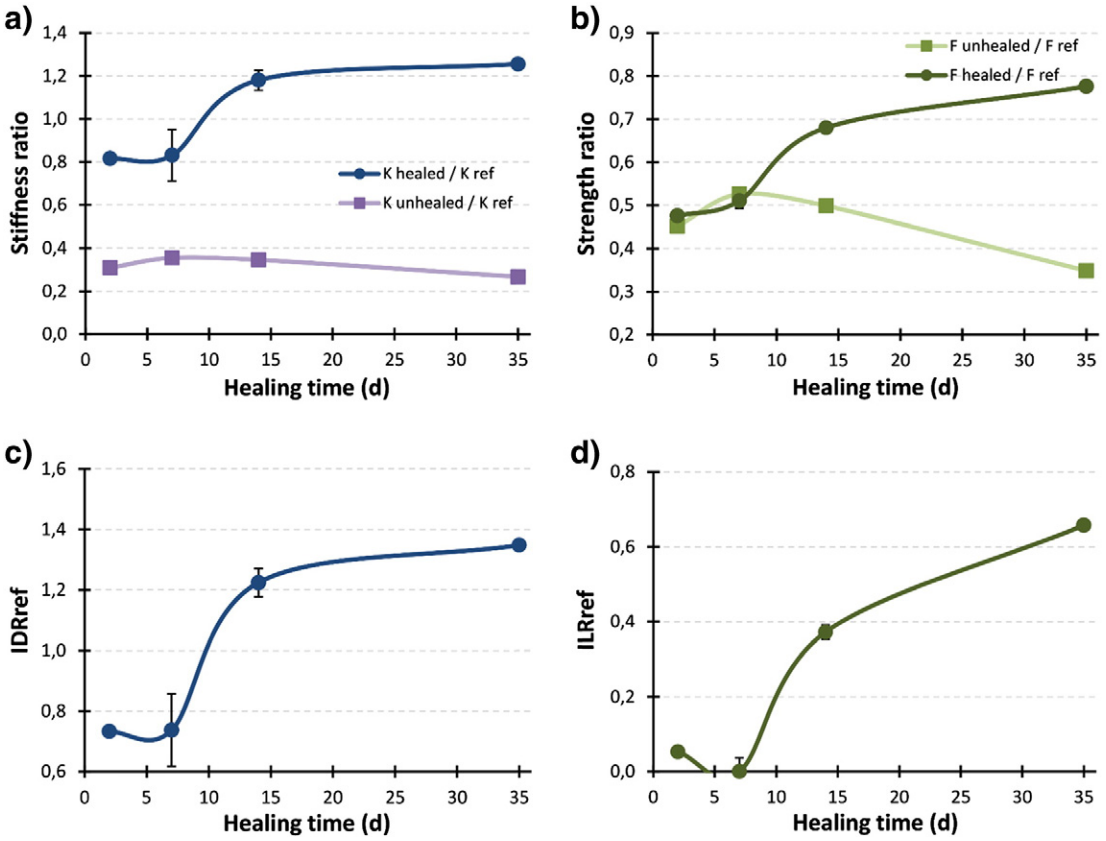

Fig. 8. Influence of the healing time for specimens cracked at 24 h with a 10-µm wide crack on a) stiffness regain, b) the bending strength regain, c) the index of damage recovery and, d) the index of load recovery.

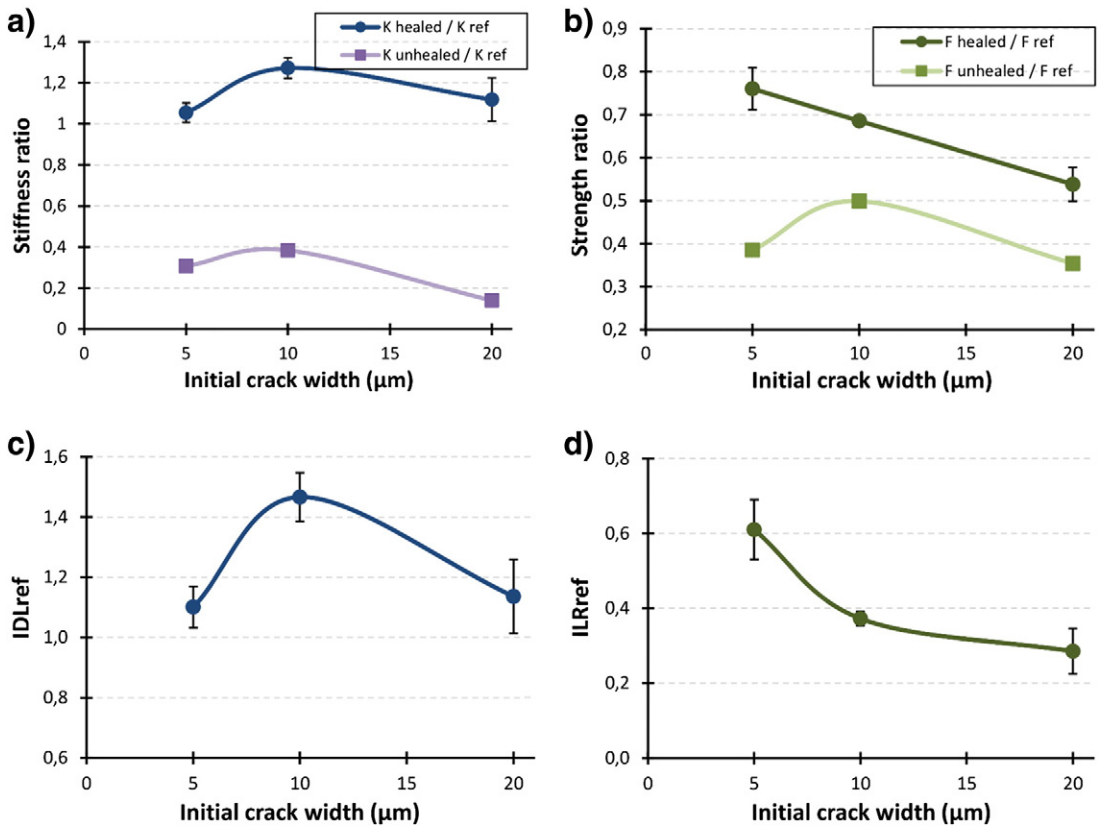

Fig 9. Influence of the initial crack width for specimens cracked at 24 h on a) stiffness regain, b) the bending strength regain, c) the index of damage recovery and, d) the index of load recovery.

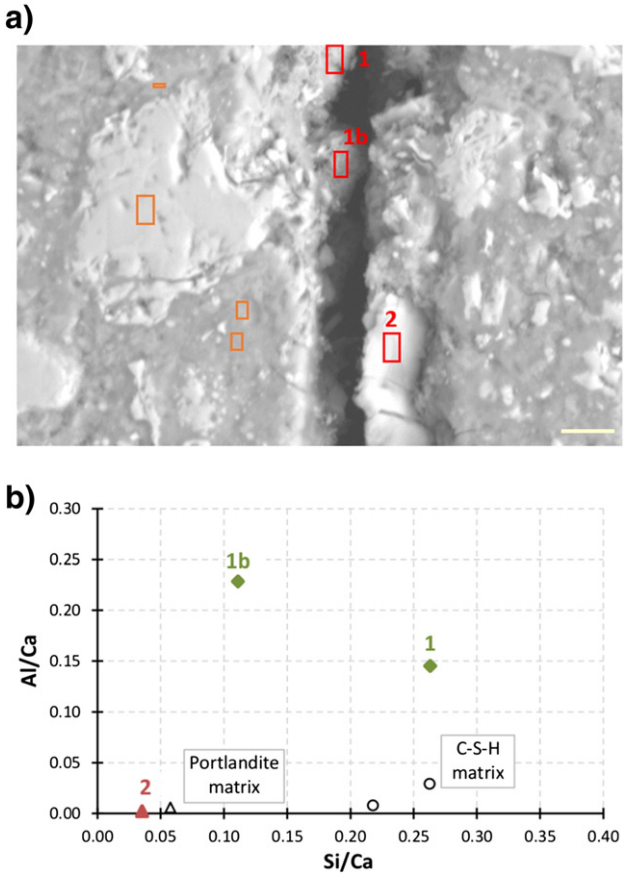

Fig. 10. SEM/EDX analysis of an artificial crack after 2 days of healing: a) BSE image (scale bar corresponds to 10 μm), b) Al/Ca vs Si/Ca plot comparing the composition of healing products and hydration products from the matrix in selected regions.

CSH occurs gradually during the first weeks for narrow cracks created before 7 days which can explain the strength regains developing with the same kinetics. On the other hand, the quick precipitation of some ettringite (and eventually portlandite and CA(S)H phases), can be responsible of the early stiffness regains observed. The stiffness regains can also possibly be attributed to some isolated fast growing CSH to a lower extent.

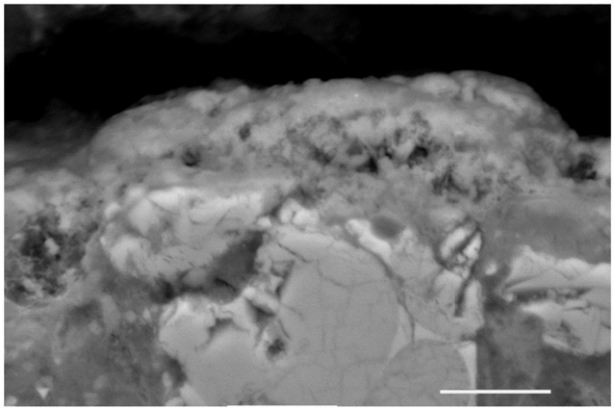

Fig. 11. Precipitation of CSH healing product nearby an anhydrous phase in an artificial crack created at 7 days (scale bar corresponds to 10 μm).

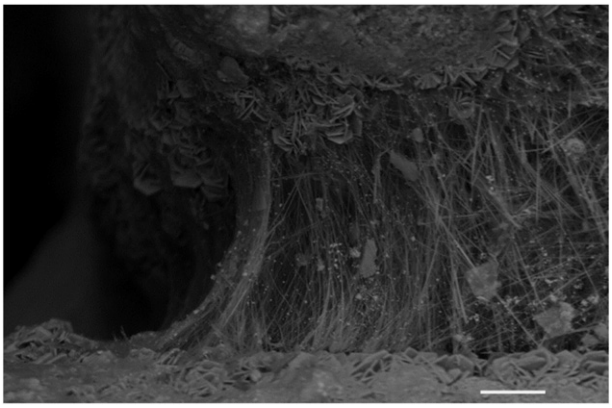

Fig. 12. Long needles bridging the crack surface of early age cracked cement paste (scale bar corresponds to 50 μm).

4.3. Discussion on the self-healing results based on modelling considerations

4.3.1. Influence of the age at cracking and of the healing period

The development of a microstructural model supplements experiments. On the one hand by studying very small cracks which are relatively hard to create and monitor in laboratory samples. On the other hand by giving access to local mechanical properties along different directions. In this study, major experimental results concerning healing potential and speed can be predicted by the model. For 10-μm wide cracks, only the one created at 24 h can heal within a relatively short period of some weeks (see Fig. 13a). Both mechanical regains for cracks created at 72 h and 7 days remain close to 0 even after a long healing period equivalent to 10–20 weeks. As mechanical regains in the model appear as soon as a bridge of hydrates crosses the crack, this means that no bridge is created in the volume submitted to mechanical tensile test. For the 10-μm wide crack created at 24 h, the first mechanical regains due to healing by ongoing hydration appear

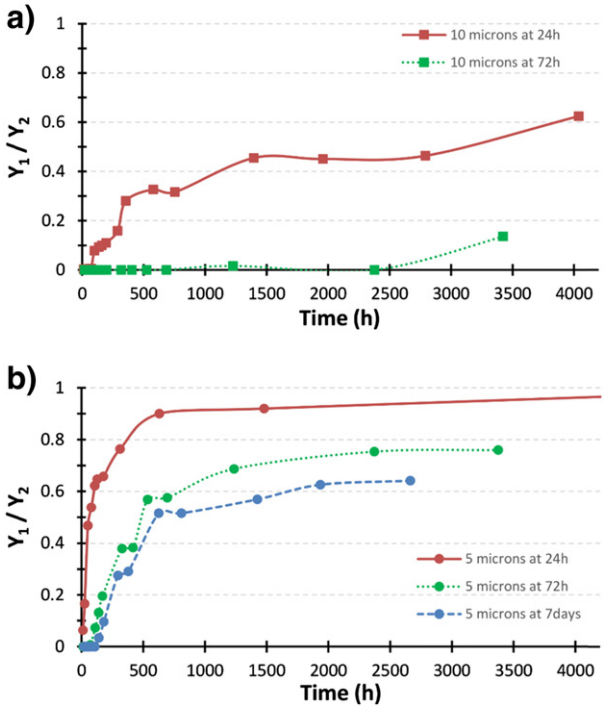

Fig. 13. Mechanical regains vs healing time and age of cracking a) for a 10-μm wide crack and b) for a 5-μm wide crack.

around 100 h and increase considerably around 300 h which is in agreement with the experimental bending capacity regains which occur between 1 and 2 weeks. The very fast experimental stiffness regain occurring before 2 days (Fig. 8a) can be explained by the quick filling of the crack [22] especially with small particles which are not described by CEMHYD3D discretisation or which have poor mechanical properties [43]. Therefore, bridges responsible for stiffness regains can appear before the mechanical regains predicted by the model due to hydrated particles smaller than 1 µm. Moreover, experimental stiffnesses reported are calculated based on load vs CMOD curves and stiffness calculated from load vs deflection curves could have a different trend. For this reason, most of the following results from the model will be discussed in regards to the experimental bending capacity regains.

In order to better understand the influence of the age at cracking and the healing period duration, the focus has been made on the healing of 5-µm wide cracks. Such narrow cracks are relatively hard to obtain experimentally but their study can be interesting to better understand the initiation of early age shrinkage cracks. The earlier the crack is created, the faster the first mechanical regains appear and the higher the healing potential (Fig. 13b). Almost complete mechanical regains can be obtained when the cracks are created at 24 h. These cracks can also heal quickly as the maximal mechanical regains are almost reached after 500 h (20 days). Thus the model agrees well with the experimental results presented in parts 4.1.1 and 4.1.2.

4.3.2. Influence of the crack width

The initial crack width determines the healing potential, e. g. the maximal mechanical regains. While healing of 10-µm wide cracks proceeds almost stepwise with the creation of a relatively small number of bridges at a low speed, the healing process of a 5-µm wide crack is faster and can occur within the first 50 h (Fig. 14a). The trend of the mechanical regains associated with a 5-µm wide crack can be explained by the transition between the surface-controlled process and the diffusion-controlled process. While there are unhydrated clinkers on the crack lips, they tend to dissolve quickly (Fig. 14b) and precipitate nearby as they seed on a solid, making the creation of the bridges over the crack relatively easily. However, for 10-µm wide cracks, the crack filling process slows down before the creation of bridges. Then the mechanical regains characterising healing increase relatively slowly when they occur after around 100 h.

4.3.3. Composition and distribution of the healing products

Composition and distribution of the healing products can be computed over the entire volume of the crack and the influence of the crack healing on the matrix composition can be analysed. As observed experimentally, the healing products precipitate inside the crack from the crack lips to the centre. Thus the centre of the crack is the zone with the highest porosity. At a given age, the average CSH, high density CSH and CH content inside the matrix are almost constant far from the crack. But close to the crack a higher volume of CSH and CH precipitates while almost no high density CSH is produced due to the reaction of anhydrous clinker present at crack formation which reacts with the water coming from the crack, as illustrated in Fig. 15a.

Inside the crack, the major healing product is CH as it has been observed in other studies for mortar at the age of 7 days [22]. The average ratio over the whole crack between CSH and CH volume fraction for a 10-µm crack is around 0.37 as illustrated by Fig. 15b. This value, in good agreement with experimental values [22], is much smaller than the ratio in the matrix (mean over all the voxels situated at least at 10 µm from the crack lips) which is around 2.5–3 for this formulation. The ratio CSH/CH decreases drastically to around 0.06 in the centre of the crack. All the CSH/CH ratios remain approximately constant over the healing period in the model. This result can be correlated with the constant stoichiometry of the hydration reactions and should be adapted to describe portlandite/calcite precipitation due to the reaction between water filling the crack and matrix, especially if one would use such a model for permeability prediction. The model also leads to the precipitation of ettringite and CAH phases into the crack due to C_3A and C_4AF hydration, which corroborates the SEM/EDX experimental observation of some high aluminium proportion in some early age healing products as presented in part 4.2.

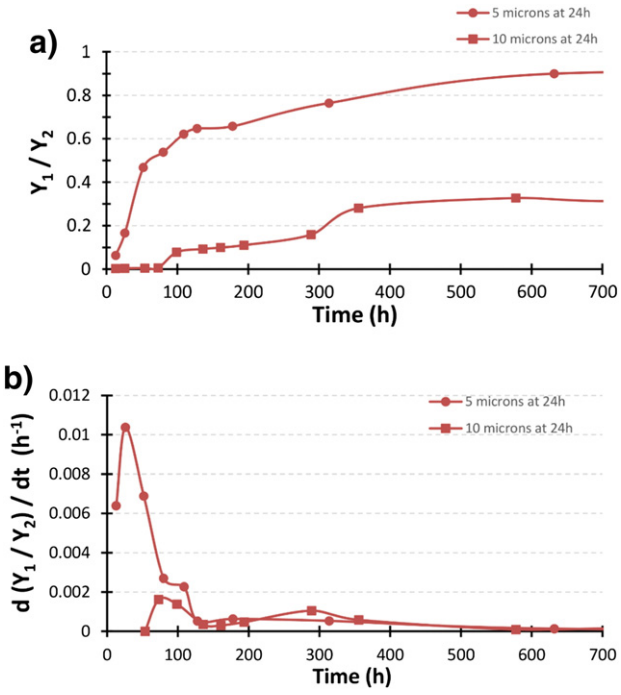

Fig. 14. Influence of the crack width on a) the mechanical regains predicted by the model and b) speed of the mechanical regain.

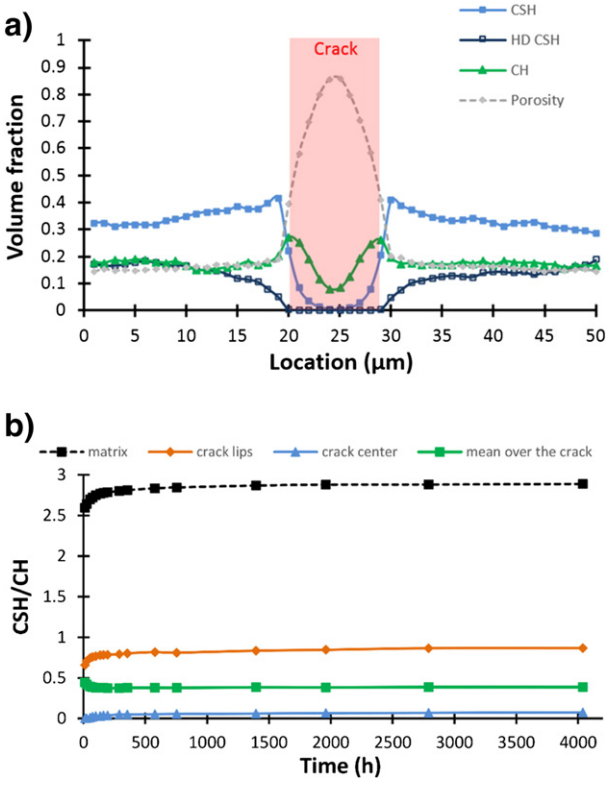

Fig. 15. Composition and distribution of the healing products a) spatially perpendicular to the crack and, b) volume ratio of CSH and CH evolution at different locations.

Finally, a rather good correlation, in terms of speed and initial starting date, can be made between the mechanical regains and the filling fraction evolution due to hydration products in the centre of the crack, as illustrated by Fig. 16a. One can observe that mechanical regains are quantifiable when the crack filling fraction is around 10% at approximately 50 h, and, for longer healing periods, the mechanical regains are proportional to crack bridging (Fig. 16b). With the assumption that the healing is symmetric on the two crack lips and the healing product mechanical properties are constant, the mechanical regains can be directly correlated to the hydration products filling fraction in the middle of the crack: the mechanical regains can appear quickly after 50–100 h and their evolution is rather fast during the first 500 h while there is still a consequent amount of hydrates precipitating into the crack creating bridges.

5. Conclusion and perspectives

In this study, a quantification of the healing capacity and kinetics of low water to cement ratio concrete cracked at early age, has been proposed both experimentally and numerically. The results show that very good mechanical regains can be obtained within 2 weeks, both in terms of stiffness and bending strength for relatively small cracks with a width of less than 10 μm when they are created before 72 h. Thus, concrete structures subjected to premature cracking can heal with mechanical regains while immersed into water. We showed that the analysis of three-point bending curves is a powerful tool to assess the behaviour of the healing products. Their different shapes reveal gradual regains both in terms of stiffness and strength, the former preceding the later. In case of two-slopes behaviour, we showed that the influence of the healing products is predominant in the first slope as predicted by a model we previously developed [43]. According to the SEM/EDX observation of artificially cracked cement paste at early age, the gradual strength regains can be attributed to the development of portlandite and CSH, while the faster stiffness regains are most probably due to the quick formation of ettringite and CA(S)H phases as well as small quantities of portlandite and CSH which could locally bridge the crack. While many improvements still need to be done concerning modelling of self-healing, the complementary development of a micro-mechanical model gives encouraging information. The finite element analysis performed with Cast3M based on output maps of the hydration model CEMHYD3D revealed that the mechanical regains can be attributed to the development of microstructural bridges between the crack lips. These bridges, mainly composed of portlandite, and in a smaller extent of CSH, ettringite and CAH, can appear very quickly for small cracks within the first dozens of hours, following the fast filling of the crack [22]. However, for larger cracks or cracks created after 72 h, the healing potential is considerably decreased and the healing phenomenon is slower because of the lack of remaining unhydrated products.

Several applications of the model could be developed, in addition with experimental measurements and observations in terms of concrete composition influence, to better understand the natural healing phenomenon. For later cracking or larger cracks, development of reactive transports models based on diffusion of ions outside the matrix, 'carbonation' reactions due to the environment could be of interest for impermeability preoccupations, even though mechanical regains are much more limited [54]. All these studies could help determining the natural healing capacity of a given concrete and consequently design autonomous healing systems to increase or complete this ability.

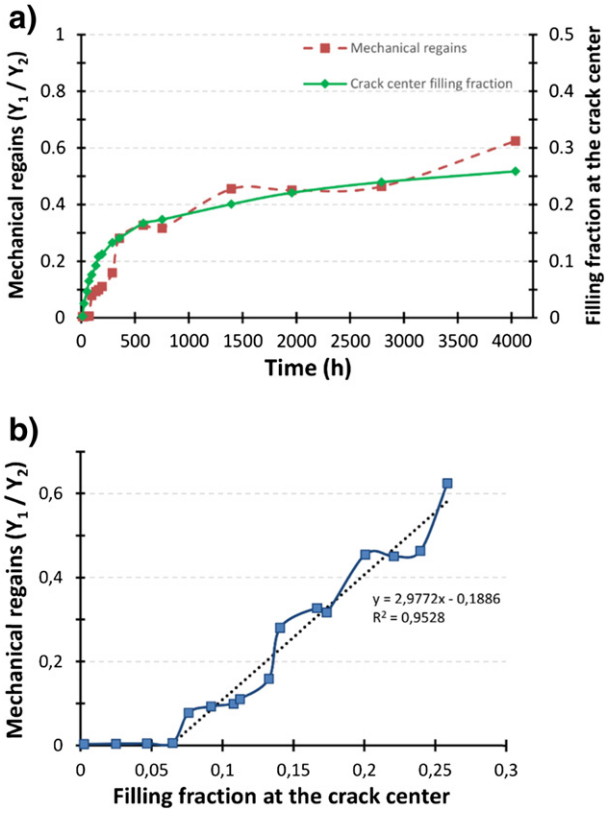

Fig. 16. Numerical mechanical regains due to the crack healing and filling fraction in the centre of the crack: a) as a function of the healing time, b) the former vs. the latter (with the best fitting affine regression for mechanical regains values greater than 0).

Acknowledgments

The authors gratefully acknowledge the financial support provided for this study by GIS LIRGeC and France's Loire Valley Regional Council. The authors acknowledge the cooperation of Mrs. Annabelle Defrance in performing experimental tests in partial fulfilment of the requirements for the engineering programme of the Ecole Polytech Montpellier. Special thanks are due to Elke Gruyaert, Anass Cherki El Idrissi, Jeroen Dils and Mieke De Schepper for their help performing calorimetric and laser diffraction measurements as well as Yannick Benoit for his technical assistance during SEM/EDX measurements. D.P. Bentz and E.J. Garboczi are acknowledged for CEMHYD3D hydration model and V. Šmilauer for CemPy.

References

[1] K. van Breugel, Self-healing concepts in civil engineering for sustainable solutions: potential and constraints, Proceedings of the Second International Conference on Self-Healing Materials, 2009.
[2] M. de Rooij, K. Van Tittelboom, N. De Belie, E. Schlangen (Eds.), Self-Healing Phenomena in Cement-Based Materials, Springer, Netherlands, 2013.
[3] L. Ferrara, V. Krelani, M. Carsana, A 'fracture testing' based approach to assess crack healing of concrete with and without crystalline admixtures, Constr. Build. Mater. 68 (2014) 535–551.
[4] C. Dry, Matrix cracking repair and filling using active and passive modes for smart timed release of chemicals from fibers into cement matrices, Smart Mater. Struct. 3 (1994) 118–123.
[5] B. Hilloulin, K. Van Tittelboom, E. Gruyaert, N. De Belie, A. Loukili, Design of polymeric capsules for self-healing concrete, Cem. Concr. Compos. 55 (2015) 298–307.
[6] M.M. Pelletier, R. Brown, A. Shukla, A. Bose, Self-Healing Concrete with a Microencapsulated Healing Agent2015.
[7] K. Van Tittelboom, N. De Belie, D. Van Loo, P. Jacobs, Self-healing efficiency of cementitious materials containing tubular capsules filled with healing agent, Cem. Concr. Compos. 33 (4) (2011) 497–505.
[8] H. Jonkers, Bacteria-based self-healing concrete, Heron 56 (2011) 1–12.
[9] J. Wang, H. Soens, W. Verstraete, N. De Belie, Self-healing concrete by use of microencapsulated bacterial spores, Cem. Concr. Res. 56 (2014) 139–152.
[10] V. Wiktor, H.M. Jonkers, Quantification of crack-healing in novel bacteria-based self-healing concrete, Cem. Concr. Compos. 33 (7) (2011) 763–770.
[11] V.C. Li, Y.M. Lim, Y.-W. Chan, Feasibility study of a passive smart self-healing cementitious composite, Compos. Part B 29 (6) (1998) 819–827.
[12] T. Nishiwaki, S. Kwon, D. Homma, M. Yamada, H. Mihashi, Self-healing capability of fiber-reinforced cementitious composites for recovery of watertightness and mechanical properties, Materials 7 (3) (2014) 2141–2154.

[13] K. Sisomphon, O. Çopuroglu, E. Koenders, Effect of exposure conditions on self healing behavior of strain hardening cementitious composites incorporating various cementitious materials, Constr. Build. Mater. 42 (2013) 217–224.
[14] Y. Yang, M.D. Lepech, E.-H. Yang, V.C. Li, Autogenous healing of engineered cementitious composites under wet–dry cycles, Cem. Concr. Res. 39 (5) (2009) 382–390.
[15] Y. Yang, E.-H. Yang, V.C. Li, Autogenous healing of engineered cementitious composites at early age, Cem. Concr. Res. 41 (2) (2011) 176–183.
[16] B. Hilloulin, Y. Zhang, O. Abraham, A. Loukili, F. Grondin, O. Durand, V. Tournat, Small crack detection in cementitious materials using nonlinear coda wave modulation, NDT and E Int. 68 (2014) 98–104.
[17] C.-W. In, R.B. Holland, J.-Y. Kim, K.E. Kurtis, L.F. Kahn, L.J. Jacobs, Monitoring and evaluation of self-healing in concrete using diffuse ultrasound, NDT and E Int. 57 (2013) 36–44.
[18] E. Tsangouri, D.G. Aggelis, K. Van Tittelboom, N. De Belie, D. Van Hemelrijck, Detecting the activation of a self-healing mechanism in concrete by acoustic emission and digital image correlation, The Scientific World Journal, 2013.
[19] K. Van Tittelboom, N. De Belie, F. Lehmann, C. Grosse, Use of acoustic emission analysis to evaluate the self-healing capability of concrete, Nondestructive Testing of Materials and Structures, vol. 6 of RILEM Bookseries, Springer Netherlands2013 51–57.
[20] C. Edvardsen, Water permeability and autogenous healing of cracks in concrete, ACI Mater. J. 96 (4) (1999) 448–454.
[21] N. Hearn, Self-sealing, autogenous healing and continued hydration: what is the difference? Mater. Struct. 31 (8) (1998) 563–567.
[22] H. Huang, G. Ye, D. Damidot, Characterization and quantification of self-healing behaviors of microcracks due to further hydration in cement paste, Cem. Concr. Res. 52 (2013) 71–81.
[23] B. Hilloulin, F. Grondin, A. Loukili, O. Abraham, Cinétique et potentiel d'autocicatrisation des matériaux cimentaires: expériences et modèle de transport réactif, Proceedings of 32nd Rencontres Universitaire de Génie Civil, 2014 (AUGC 2014).
[24] K. Lauer, F. Slate, Autogenous healing of cement paste, Am. Concr. Inst. J. 52 (1956) 1083–1097.
[25] Y. Abdel-Jawad, R. Haddad, Effect of early overloading of concrete on strength at later ages, Cem. Concr. Res. 22 (5) (1992) 927–936.
[26] R.K. Dhir, C.M. Sangha, J.G.L. Munday, Strength and deformation properties of autogeniously healed mortars, J. ACI 70 (1973) 231–236.
[27] S. Jacobsen, E.J. Sellevold, Self healing of high strength concrete after deterioration by freeze/thaw, Cem. Concr. Res. 26 (1) (1996) 55–62.
[28] S. Granger, Caractérisation expérimentale et modélisation du phénomène d'autocicatrisation des fissures dans les bétons, Ph.D. thesis, Ecole Centrale de Nantes, 2006.
[29] S. Granger, A. Loukili, G. Pijaudier-Cabot, G. Chanvillard, Experimental characterization of the self-healing of cracks in an ultra high performance cementitious material: mechanical tests and acoustic emission analysis, Cem. Concr. Res. 37 (4) (2007) 519–527.
[30] K. Van Tittelboom, E. Gruyaert, H. Rahier, N. De Belie, Influence of mix composition on the extent of autogenous crack healing by continued hydration or calcium carbonate formation, Constr. Build. Mater. 37 (2012) 349–359.
[31] N. Ter Heide, Crack Healing in Hydrating Concrete, Delft University of Technology, Master's thesis, 2005.
[32] D.P. Bentz, Three-dimensional computer simulation of portland cement hydration and microstructure development, J. Am. Ceram. Soc. 80 (1) (1997) 3–21.
[33] F. Bernard, S. Kamali-Bernard, W. Prince, 3d multi-scale modelling of mechanical behaviour of sound and leached mortar, Cem. Concr. Res. 38 (4) (2008) 449–458.
[34] C.-J. Haecker, E. Garboczi, J. Bullard, R. Bohn, Z. Sun, S. Shah, T. Voigt, Modeling the linear elastic properties of portland cement paste, Cem. Concr. Res. 35 (10) (2005) 1948–1960.
[35] H. He, Z.-Q. Guo, P. Stroeven, J. Hu, M. Stroeven, Computer simulation study of concrete's self-healing capacity due to unhydrated cement nuclei in interfacial transition zones, Proceedings of the First International Conference on Self Healing Materials, 2007.
[36] H. He, Z. Guo, P. Stroeven, M. Stroeven, Numerical assessment of concrete's self-healing potential for promoting durability, Int. J. Model. Identif. Control. 7 (2009) 142–147.
[37] Z. Lv, H. Chen, Modeling of self-healing efficiency for cracks due to unhydrated cement nuclei in hardened cement paste, Proc. Eng. 27 (2012) 281–290.
[38] Z. Lv, H. Chen, Self-healing efficiency of unhydrated cement nuclei for dome-like crack mode in cementitious materials, Mater. Struct. (2013) 1–12.
[39] H. Huang, G. Ye, Simulation of self-healing by further hydration in cementitious materials, Cem. Concr. Compos. 34 (4) (2012) 460–467.
[40] H. Huang, G. Ye, D. Damidot, Effect of blast furnace slag on self-healing of microcracks in cementitious materials, Cem. Concr. Res. 60 (2014) 68–82.
[41] C. Joseph, A.D. Jefferson, R.J. Lark, Lattice modelling of autonomic healing process in cementitious materials, Proceedings of the 8th. World Congress on Computational Mechanics (WCCM8) and 5th. European Congress on Computational Methods in Applied Sciences and Engineering, 2008 (ECCOMAS 2008).
[42] A. Caggiano, L. Ferrara, V. Krelani, G. Etse, Zero-thickness interface formulation for fracture analysis of self-healing concrete, in: S. Idelsohn, et al., (Eds.), Proceedings 1st Pan American Congress on Computational Mechanics and XI Argentine Congress on Computational Mechanics 2015, pp. 553–564.
[43] B. Hilloulin, F. Grondin, M. Matallah, A. Loukili, Modelling of autogenous healing in ultra high performance concrete, Cem. Concr. Res. 61 (2014) 64–70.
[44] G. di Luzio, L. Ferrara, V. Krelani, A numerical model for the self healing capacity of cementitious composites, Proceedings Euro-C 2014, Computational Modelling of Concrete and Concrete Structures 2014, pp. 741–774.
[45] F. Grondin, M. Bouasker, P. Mounanga, A. Khelidj, A. Perronnet, Physico-chemical deformations of solidifying cementitious systems: multiscale modelling, Mater. Struct. 43 (1–2) (2010) 151–165.
[46] P. Verpaux, T. Charras, A. Millard, Castem 2000: une approche moderne du calcul des structures, in: J.M. Fouet, P. Ladevèze, R. Ohayon (Eds.),Calcul des Structures et Intelligence Artificielle 1988, pp. 261–271.
[47] V. Smilauer, Manual for cempy, ver. 0.15. http://concrete.fsv.cvut.cz/~wilson/Software/manual_0.15.pdf.
[48] O. Bernard, F.-J. Ulm, E. Lemarchand, A multiscale micromechanics-hydration model for the early-age elastic properties of cement-based materials, Cem. Concr. Res. 33 (9) (2003) 1293–1309.
[49] A. Boumiz, D. Sorrentino, C. Vernet, F. Cohen Tenoudji, Modelling the development of the elastic moduli as a function of the degree of hydration of cement pastes and mortars, Proceedings 13 of the 2nd RILEM Workshop on Hydration and Setting: Why does cement set? An interdisciplinary approach, edited by A. Nonat (RILEM, Dijon, France, 1997), 1997.
[50] K. Velez, S. Maximilien, D. Damidot, G. Fantozzi, F. Sorrentino, Determination by nanoindentation of elastic modulus and hardness of pure constituents of portland cement clinker, Cem. Concr. Res. 31 (4) (2001) 555–561.
[51] G. Constantinides, F.-J. Ulm, The effect of two types of c-s-h on the elasticity of cement-based materials: results from nanoindentation and micromechanical modeling, Cem. Concr. Res. 34 (2004) 67–80.
[52] P.J.M. Monteiro, C.T. Chang, The elastic moduli of calcium hydroxide, Cem. Concr. Res. 25 (1995) 1605–1609.
[53] R. Mills, V.M.M. Lobo, Self-diffusion in Electrolyte Solutions: A Critical Examination of Data Compiled from the Literature, 1989.
[54] B. Hilloulin, F. Grondin, A. Soive, A. Loukili, Investigation of self-healing phenomenon by calcite precipitation using reactive transport modelling and microscopic observation, Proceedings of the 15th Euroseminar on Microscopy Applied to Building Materials, 2015.